Biomass Conversion and Biorefinery (2022) 12:501–514
https://doi.org/10.1007/s13399-021-01387-z

ORIGINAL ARTICLE

Evaluation of orange and potato peels as an energy source: a comprehensive study on their pyrolysis characteristics and kinetics

Korkut Açıkalın [1]

Received: 23 December 2020 / Revised: 31 January 2021 / Accepted: 15 February 2021 / Published online: 22 February 2021

Abstract

The orange and potato peels can be evaluated as raw materials in pyrolysis process to produce sustainable fuels and chemicals. The present study focuses on determining pyrolysis characteristics and kinetics of orange and potato peels. Thus, thermogravimetric analyses of said peels were studied from ambient temperature to 650°C at 2, 10 and 15°C/min heating rates under N_2 atmosphere. The studies revealed that the thermal decomposition of orange peels occurs in four stages whereas potato peels decompose in three stages. The second and third stages of orange peel pyrolysis and the second stage of potato peel pyrolysis were determined as active pyrolysis stages. The kinetic parameters of active pyrolysis stages were calculated by direct Arrhenius plot, Coats-Redfern, Friedman and Kissinger-Akahira-Sunose methods. The average activation energies calculated by all methods were relatively in good agreement for second stages, but the same cannot be said for the third stage of orange peel pyrolysis. Considering the conversion values based on volatiles and the calculated average activation energy values, the orange and potato peels were projected to be valuable and sustainable energy sources which can be evaluated by pyrolysis process.

Keywords Orange peel · Potato peel · Pyrolysis kinetics · Model-fitting methods · Isoconversional methods

1 Introduction

The energy demand throughout the world persistently increases mainly due to the increase in population and evolution of industry. Speaking in terms of numbers, the population of world has increased about two billion in only one generation [1], and the world economy has advanced approximately 2.5 times in terms of gross domestic product (GDP) compared to three decades earlier [2]. This progression has been achieved by providing considerable amounts of additional energy resources. It is obvious that the upcoming years will compel the burden on energy need, with an estimation of 30% global energy demand increment in 2035 [3].

Biomass is an abundant, locally grown, renewable, sustainable and environmentally friendly alternative source of energy. Thus, it is being considered as one of the most promising alternatives to fossil fuels. Currently, biomass contributes between 10 and 14% of the global energy supply [4], and demonstrates an increasing rate of 2.5% per year [5]. Hence, it may be concluded that biomass still counts for a relatively small portion of world's total energy demand, and has a great potential to provide much more of the energy needed throughout the world.

Thermochemical conversion processes are probably the most common methods to convert biomass into energy, fuel and/or chemicals. Pyrolysis process, which can be defined as the thermal degradation of biomass in an oxygen-free environment, is a thermochemical process and is of great importance since it allows production of liquid, solid and gaseous products from biomass as well as being a first step of other thermochemical conversion processes (i.e. direct combustion and gasification). Pyrolysis is considered as a promising technology in which wastes can be converted into liquid fuels with higher liquid yields [6]. Pyrolysis process is basically affected by the properties of biomass subjected to pyrolysis and a number of process parameters applied during the process. For this reason, it is essential to understand pyrolysis behaviour of any kind of biomass in order to provide an efficient and optimized pyrolysis process. Biomasses cannot be fed to any commercial thermal plant without providing a clear understanding of the pyrolytic conditions [7]. Moreover, a

✉ Korkut Açıkalın
korkut.acikalin@yalova.edu.tr

[1] Department of Energy Systems Engineering, Yalova University, Çınarcık yolu üzeri, Merkez Yerleşke, B Blok, 77200 Yalova, Turkey

comprehensive understanding of pyrolysis kinetics is also required to design processes [8], to make feasibility assessments and to upscale the processes to industry [9]. Kinetic analysis reveals important data about the reaction mechanism, and mathematical models describing the process can be established [10].

Thermogravimetric analysis (TGA) is a commonly used technique for determination of pyrolytic behaviours and studying the kinetics of biomass samples. TGA is generally carried out either isothermally or non-isothermally for kinetic evaluations. Non-isothermal TGA is usually preferred over isothermal one since it is assumed to be simpler and it requires fewer experiments [11]. Model-fitting and model-free (or isoconversional) methods are two common kinetic methods used to calculate kinetic parameters from non-isothermal TGA data. In model-fitting method, several reaction models are considered to describe the pyrolysis of solid biomass and the model giving the best statistical fit is selected as the reaction model from which kinetic parameters are calculated. On the other hand, model-free methods do not require selection of a reaction model and consist of generating several kinetic curves at different heating rates from which activation energies are calculated isoconversionally. Both methods have their own benefits, and they are complementary rather than being competitive [12]. It should also be mentioned that not all model-free methods are isoconversional. An example covering this statement is Kissinger method. Kinetics methods are also subdivided into differential or integral categories. The differential isoconversional methods use instant rate values which makes them sensitive to experimental noise. However, integral methods do not involve this issue especially in TGA experiments [13]. Apart from model-fitting and model-free methods, NLR (nonlinear regression) is another option that can be used in calculation of kinetic parameters. This method allows a direct fit of the model to experimental data without any transformation [14].

Orange (*Citrus sinensis*, family Rutaceae) [15] was reported as the most abundant fruit crop with 73.31 million tonnes global production rate in 2017. Top producers were Brazil, China and USA actualizing almost 40% of total production [16]. Orange peel (OP) is a biomass waste material which arises mainly from orange juice, soft drink, jam industries and freshly eaten orange fruits. The solid waste generated during juice and jam process is about 50–60% by weight of the fruit [17] and consists 60–65 wt% peels [18]. Generally, this huge amount of waste is spread on soil in areas adjacent to the production sites, or used as a raw material in producing animal feed, or else is burned [19]. However, the high energy demand of dehydration process, its bitterness and low nutritional value are main drawbacks when animal feeding is concerned. Moreover, landfilling is not encouraged and should be minimized according to the requirements of the EU landfilling directive [20]. Combustion is also not an efficient way of evaluation due to the substantial moisture content. On the other hand, orange peels are known to be mostly composed of hemicellulose, cellulose, pectin, lignin, chlorophyll pigments and other low molecular weight hydrocarbons [21]. Thus, they have the potential of being utilized as an energy source by converting them into valuable fuels/products via pyrolysis process.

Potato (*Solanum tuberosum* L.) is the fourth most grown agricultural product in the world and has great importance in terms of feeding and economy [22]. The global potato production in 2016 was estimated as 376 million tonnes [23]. Potato is generally evaluated in food processing industry such as chip, crisp, instant potato, starch production, fast-food sector, and consumed freshly in domestic use. Potato peel (PP) (i.e. the skin/shell covering potato) is the basic waste unavoidably generated regardless of evaluation type. The peels discarded as waste can be 12% of the original weight [24]. PPs are generally discarded, composted or evaluated as animal feed. Composting is known to have high cost and low added value while inert materials can cause difficulties in usage as animal feed [25]. Considering global production rate and waste amount, discarding such huge amount of waste definitely will pose serious environmental issues. Thus, more efficient, valuable and environmentally friendly way of evaluation of PPs is still of great importance. From this point of view, converting PP wastes by pyrolysis to valuable fuels and/or products may be a promising option to be considered since they seem to be candidate raw material for pyrolysis process based on the fact that they are composed of starch, hemicellulose, cellulose, lignin and fermentable sugars [26].

Pyrolysis kinetics of OP was studied by limited number of researchers. In one study [10], kinetic parameters of OP pyrolysis were calculated by five different model-free methods (Kissinger-Akahira-Sunose (KAS), Flynn-Wall-Ozawa (FWO), Starink, Vyazovkin and Friedman) and one model-fitting (distributed activation energy model–DAEM) method. In another study [27], activation energies of OPs were determined by using model-free Kissinger method. De Morais et al. [28] used Ozawa-Flynn-Wall method to calculate activation energy of OPs. FWO, KAS and Kissinger methods were also used in kinetic study of catalytic pyrolysis process of sweet orange peels [29]. Kinetic study of orange pulp pyrolysis was also carried out by using Friedman and KAS methods [30]. Ozawa method was another model-free method used in kinetic study of OP pyrolysis [31]. Having examined the abovementioned studies, it can be seen that all the kinetic studies related to OPs were carried out using various model-free methods, except one, in which DAEM method was used as the sole model-fitting method. It was noticed that the common model-fitting methods such as Coats-Redfern, direct Arrhenius plot were not used to calculate kinetic parameters of OP pyrolysis. Moreover, a few numbers of pyrolysis studies of PP [32–34] were noted during the literature search; however, to the best of author's knowledge, a kinetic study on pyrolysis of PP was not reported yet.

The present study was conducted to fulfil the lack of information in the field of OP and PP pyrolysis kinetics which were noticed during the literature review. For this purpose, OP and PP were subjected to TGA under pyrolytic conditions. The kinetic parameters, namely, activation energy, reaction order and pre-exponential factor, were calculated by using either model-fitting or model-free methods including both differential and integral ones. Thus, a mandatory initial step needed to design, optimize and upscale the pyrolysis process of OP and PP, was accomplished by calculating the kinetic parameters of OP and PP pyrolysis comparatively and comprehensively.

2 Materials and methods

2.1 Materials

The potato and oranges were supplied from a local market place located at the city centre of Yalova (Turkey). The samples were washed with tap water to ensure the removal of any dirt, soil or other impurities. Next, the orange and potato samples were peeled. The obtained peel samples (OPs and PPs) were pre-dried at ambient temperature under air atmosphere approximately for a period of 1 week. The pre-dried samples were ground to particle size of <0.2mm by using an analytic mill. The final drying process of samples was established in an oven at 105°C for 2 h. The samples were stored in air-tight dark brown glass containers placed in moisture-free shelves which were not exposed to sunlight. The ash, moisture and volatile matter contents were determined accordingly to ASTM D1102-84-2013, ASTM E871-82-2013 and ASTM D1762-84-2013 standards, respectively. The elemental analysis and higher heating value of samples were determined by using an elementary analyser (LECO CHNS-932, USA) and a bomb calorimeter (IKA C5000, Germany), respectively. The proximate and ultimate analyses of peel samples were performed over the milled and dried biomass. The results are presented in Table 1.

Table 1 Proximate and ultimate analyses results of OP and PP

Analysis	OP	PP
Proximate analysis (wt%)		
Moisture content	12.84	8.07
Volatile matter	70.51	68.80
Ash content	2.60	8.75
Fixed carbon[a]	14.05	14.38
Ultimate analysis (wt%)		
C	44.51	43.94
H	5.99	6.08
O[a]	48.20	47.20
N	1.08	2.78
S	0.22	-
HHV[b] (MJ/kg)	18.32	17.36

[a] By difference, [b] Higher heating value

2.2 TGA

The data needed to study pyrolysis characteristics and kinetics of OP and PP were obtained from non-isothermal TGA measurements carried out from ambient temperature to 650°C at heating rates of 2, 10 and 15°C/min under 50 ml/min flowrate of N_2 gas by using EXSTAR SII TG/DTA 6300 (Seiko Instruments, Japan) model thermogravimetric analyser. The average amount of sample used in the experiments was approximately 7 mg.

2.3 Kinetic theory

Devolatilization is a basic step of all thermochemical processes and involves the release of volatiles as the chemical bonds of biomass constituents, i.e. hemicellulose, cellulose, lignin, are thermally cleaved. In reality, it has a complex mechanism composed of several consecutive and parallel chemical reactions. However, it is generally simplified to the following single reaction:

$$\text{biomass} \rightarrow \text{char} + \text{volatiles} \quad (1)$$

The rate of reaction is given by the linear function of reaction rate constant ($k(T)$) and reaction model ($f(\alpha)$):

$$\frac{d\alpha}{dt} = k(T)f(\alpha) \quad (2)$$

where α is conversion degree, or the fraction of pyrolyzed biomass, and is defined by the terms of m_o (the mass of biomass at the beginning), m_t (the mass of biomass at time t) and m_f (the mass of biomass at the end of event of interest) as:

$$\alpha = \frac{(m_0 - m_t)}{(m_0 - m_f)} \quad (3)$$

Equation 2 can be rewritten by inserting Arrhenius equation ($k(T) = Ae^{-\frac{E_a}{RT}}$) as:

$$\frac{d\alpha}{dt} = Ae^{-\frac{E_a}{RT}}f(\alpha) \quad (4)$$

where A, E_a, R and T are pre-exponential (or frequency) factor (time^{-1}), apparent activation energy (J/mol), gas constant (8.314 J/(mol K)) and temperature (K), respectively. For non-isothermal studying conditions, temperature is a function of time, and it increases with a constant heating rate (β) starting from an initial value (T_0) as follows:

$$T = T_0 + \beta t \quad (5)$$

Following equation is obtained by differentiating Eq. 5:

$$dT = \beta dt \quad (6)$$

Equation 6 can be rearranged as:

$$dt = \frac{dT}{\beta} \tag{7}$$

Equation 8 can be obtained by applying Eq. 7 in Eq. 4 as given below:

$$\frac{d\alpha}{dT} = \frac{A}{\beta} e^{-\frac{E_a}{RT}} f(\alpha) \tag{8}$$

Equation 8 can be rearranged by collecting the related terms at the same sides as follows:

$$\frac{d\alpha}{f(\alpha)} = \frac{A}{\beta} e^{-\frac{E_a}{RT}} dT \tag{9}$$

Equation 9 is the fundamental equation in differential form that can be used to calculate kinetic parameters from non-isothermal TGA data. Equation 9 can also be expressed in integral form by integrating it [35–37]:

$$g(\alpha) = \int_0^{\alpha} \frac{d\alpha}{f(\alpha)} = \frac{A}{\beta} \int_0^{T} e^{-\frac{E_a}{RT}} dT = \frac{AE_a}{\beta R} P(x) \tag{10}$$

where $g(\alpha)$ is the integral form of the reaction model and $x = {}^{E_a}/_{RT}$. The right side of the equation, $P(x)$, also called as the temperature integral, has no exact analytical solution. However, numerous approximation methods can be used to solve the temperature integral, and, thus, several integral equations were derived.

2.3.1 Friedman method

Friedman (FR) method is a widely used differential isoconversional method. FR equation is obtained simply by taking the natural logarithm of Eq. 9 as given below:

$$\ln\left(\beta \frac{d\alpha}{dT}\right) = \ln(Af(\alpha)) - \frac{E_a}{RT} \tag{11}$$

According to FR method (Eq. 11), $\ln\left(\beta \frac{d\alpha}{dT}\right)$ versus $\frac{1}{T}$ should be plotted at different heating rates for a constant conversion value, and then, activation energy (E_a) can be calculated from the slope ($-\frac{E_a}{R}$).

2.3.2 Kissinger-Akahira-Sunose method

KAS method is another widely used isoconversional method, but in integral form. KAS equation is obtained by introducing the approximation $P(x) = x^{-2}e^{-x}$ [36] into Eq. 10, and then taking natural logarithm as follows:

$$\ln\left(\frac{\beta}{T^2}\right) = \ln\left(\frac{AR}{E_a g(\alpha)}\right) - \frac{E_a}{RT} \tag{12}$$

According to Eq. 12, $\ln\left(\frac{\beta}{T^2}\right)$ versus $\frac{1}{T}$ should be plotted at different heating rates for a given value of conversion, and then, E_a can be calculated from the slope $\left(-\frac{E_a}{R}\right)$.

2.3.3 Direct Arrhenius plot method

Direct Arrhenius plot (DAP) method is a model-fitting differential method. DAP equation is obtained by taking natural logarithm of Eq. 9, and, then, inserting nth-order chemical reaction model ($(1-\alpha)^n$) for $f(\alpha)$ as follows:

$$\ln\left(\frac{d\alpha}{dT}\right) - n\ln(1-\alpha) = \ln(A/\beta) - \frac{E_a}{RT} \tag{13}$$

DAP method requires the plotting of $\ln\left(\frac{d\alpha}{dT}\right) - n\ln(1-\alpha)$ versus $\frac{1}{T}$ graphs accompanied with an appropriate selection of reaction order (n). Providing this necessity, $\ln\left(\frac{d\alpha}{dT}\right) - n\ln(1-\alpha)$ versus $\frac{1}{T}$ plot should give a straight line. Then, the E_a and pre-exponential factor can be calculated from the slope ($-\frac{E_a}{R}$) and intercept ($\ln(A/\beta)$) of this straight line.

2.3.4 Coats-Redfern method

Coats-Redfern (CR) method is a commonly used model-fitting integral method. CR equation is obtained by applying asymptotic series to the temperature integral in Eq. 10, neglecting higher orders terms, selecting nth-order chemical reaction model ($(1-\alpha)^n$) for $f(\alpha)$, simplifying for the assumption of $2RT/E \ll 1$ and taking the natural logarithm as follows [36]:

$$\ln\left(\frac{1-(1-\alpha)^{1-n}}{T^2(1-n)}\right) = \ln\left(\frac{AR}{\beta E_a}\right) - \frac{E_a}{RT} \quad (\text{for } n \neq 1) \tag{14}$$

$$\ln\left(\frac{-\ln(1-\alpha)}{T^2}\right) = \ln\left(\frac{AR}{\beta E_a}\right) - \frac{E_a}{RT} \quad (\text{for } n = 1) \tag{15}$$

In CR method, a straight line should be obtained by plotting left hand side of Eq. 14 or 15 versus 1/T if an appropriate value of n is selected. Then, E_a and pre-exponential factor can be calculated from the slope ($-\frac{E_a}{R}$) and intercept ($\ln\left(\frac{AR}{\beta E_a}\right)$) of this straight line.

3 Results and discussion

3.1 Proximate, ultimate analyses and heating values

Proximate analysis, ultimate analysis and heating value enable estimation of valuable information about biomass samples with regard to their application in pyrolysis process.

High amount of moisture content is expected to increase the energy demand of pyrolysis process since it must be removed at the initial stages of process. Moreover, higher moisture content can lead to liquid product having higher amount of water, which is not a desired property since it makes the liquid product inappropriate for combustion and gasification as fuel and lowers the heating value. For this reason, examining the moisture contents given in Table 1, further pre-dying of biomass samples, especially pre-drying of OP, may be considered. Volatile matter content plays an important role in pyrolysis process. It is known that higher amount of volatile matter increases bio-oil yield [38]. Moreover, higher amount of volatiles can constitute more porous structure while they are removed from the biomass during the pyrolysis process, which in turn increases the area of biomass that will further decompose. Therefore, high volatile matter content may be expected to accelerate pyrolysis process. The pyrolysis process of OP may be expected to present a slight advantage in terms of bio-oil yield and process rate since OP has 1.71% higher volatile matter content compared to PP (Table 1). As can be seen from Table 1, ash content of PP (8.75%) is significantly greater than the ash content of OP (2.60%). Higher ash content has generally the impact of lowering bio-oil yield [38]. Thus, OP may have an advantage in producing higher bio-oil yield by pyrolysis process since it has considerably less amount of ash as well as slightly higher volatile matter content.

Carbon and hydrogen are the fundamental combustible elements of fuels, and their increase is expected to result in an increase of heating value, making the fuel, both the biomass itself and the fuel produced from biomass, more valuable. From this point of view, OP and PP exhibit notably close values (Table 1), and thus, cannot provide a significant advantage against each other. Oxygen content does not favour the energy content of fuel, and an increase in oxygen content decreases the heating value. Moreover, it is also known that bio-oil produced in pyrolysis process is an oxygenated fuel similar to the original biomass it is produced from. Thus, a similar level of negativity can be mentioned in terms of oxygen content since the oxygen contents of both biomass wastes (Table 1) are close to each other. Nitrogen content of biomass is mainly important in terms of NO_x emissions resulting from combustion of original biomass or biomass derived fuels by pyrolysis. Less NO_x emissions are expected when the biomass or biomass-derived fuel has less nitrogen content. Therefore, examining the nitrogen contents given in Table 1, it can be predicted that the use of OP or OP-derived fuel by pyrolysis as an energy source will result in less NO_x emission when compared to the use of PP or PP-derived fuel by pyrolysis as an energy source. However, on the other hand, elemental analysis showed that PP did not consist measurable amounts of sulphur whereas OP had 0.22% sulphur content. Sulphur content is also important environmentally, and less SO_x emissions are expected when the biomass or biomass-derived fuels by pyrolysis contain less sulphur. Considering this, it can be predicted that the use of PP or PP-derived fuels by pyrolysis process as an energy source will contribute less to SO_x emissions when compared to the use of OP or OP-derived fuels by pyrolysis process as an energy source. It should also be noted that sulphur content of OP is still considerably lower than the sulphur content of most of the coal types.

It was expected that the heating values of both samples will be close to each other since the C, H and O contents were quite close to each other as explained in the former paragraph. However, the heating value of OP was app. 5.5% higher than that of PP (Table 1), which can be explained by the fact that OP contains significantly less ash content than PP, since ash refers to the unburned fraction of the fuel at the end of the combustion process, and its high value indicates that the unburned fraction will be more, and therefore, the energy obtained by burning the fuel will be less. It should also be noted that higher heating value of both OP and PP is considerably lower than that of fossil fuels.

3.2 Pyrolysis characteristics of OP and PP

The OP and PP samples were thermogravimetrically analysed to generate TG (thermogravimetric) and DTG (derivative thermogravimetric) curves from which pyrolysis characteristics can be examined, and the data needed to calculate kinetic parameters can be provided. Therefore, analyses were carried out from ambient temperature to 650°C at heating rates of 2, 10 and 15°C/min under 50 ml/min N_2 flowrate. The generated TG and DTG curves are presented in Fig. 1.

The structure and thermal stability of components that constitute biomasses differ from each other. Therefore, their thermal decomposition occurs at different temperature ranges and at different mass loss rates. Thereby, all the stages that occur at different mass loss rates in different temperature ranges, together, establish the entire pyrolysis process. These stages can be determined by examining the slope changes in a TG curve and the peaks of a DTG curve. Hence, TG/DTG curves obtained at 10°C/min (Fig. 1) were examined, and the information gathered about the pyrolysis characteristics of OP and PP are listed below:

- It can be said that thermal decompositions of OP and PP occur in four and three stages, respectively. Arenas et al. [10] also obtained four stage thermograms for OP which are very similar to the ones obtained in present study. The DTG curve of waste potato peel obtained in another study [39] is also very similar to the DTG curve obtained in present study.
- The masses of OP and PP continuously decrease between ambient temperature and the final temperature due to dehydration and thermal degradation of the structural

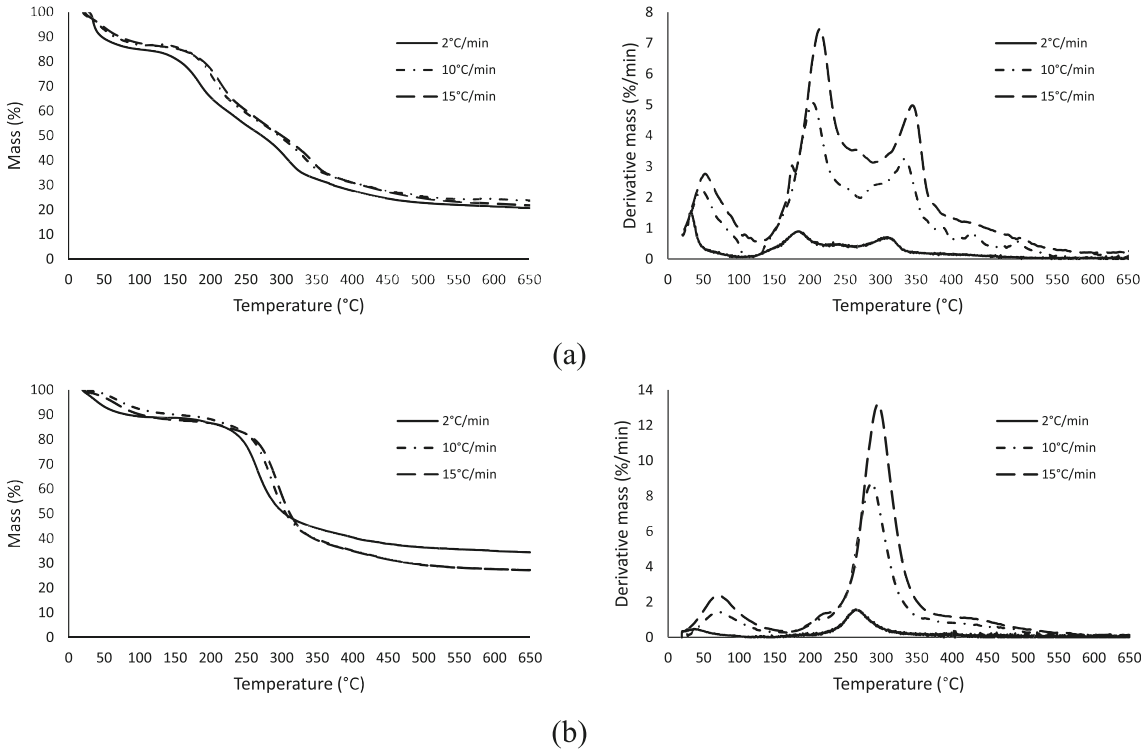

Fig. 1 TG and DTG curves for OP (**a**) and PP (**b**)

components. The first stage of OP pyrolysis took place up to 162°C with a mass loss of app. 15.1%. For PP, the first stage ended at app. 201°C with 11.9% mass loss. Mass losses of first stages can be attributed to the removal of moisture and low molecular weight volatiles. When the moisture values in Table 1 (OP: 12.84%, PP: 8.07%) are compared with the mass loss values of first stages, the larger values obtained in first stages confirm the removal of low molecular weight volatiles in addition to the moisture removal.

- Following the first stage, a dramatic increase in mass loss rates for both OP and PP can be noticed by examining the high increase at the slope of TG curves. These stages with high mass loss rates are active pyrolysis stages, and basic devolatilization reactions take place in these stages. For OP, the stage at the temperature range of 162–260°C is the second stage whereas the stage at the temperature range of 260–367°C is the third stage. These two stages together form the active pyrolysis stages for OP. Mass losses observed in these stages are 27.53% and 23.31%, respectively. For OP, the maximum mass loss rates were measured as 4.95 %/min at 208°C and 3.12 %/min at 338°C in the second and third stages, respectively. Unlike OP, the active pyrolysis stage for PP consists of a single stage, and this stage is the second stage where 39.43% mass loss occurred at the temperature range of 250–329°C. The maximum mass loss rate at this stage was 8.59 %/min, and it was measured at 290°C.
- It can be understood from the considerable decrease at the slope of TG curves that the rates of mass loss following the active pyrolysis stages were drastically decreased for both biomass waste materials. Thereby, the fourth stage of OP and the third stage of PP were the final stages of pyrolysis processes. These stages are defined as passive pyrolysis stages due to their extremely low mass loss rates. The fourth stage of OP was observed between 367 and 650°C with a mass loss of 10.32%. The third stage of PP lied between 329 and 650°C with a mass loss of 15.54%. The residual amounts of OP and PP at the end of the whole pyrolysis processes were determined as 23.64% and 27.19%, respectively.
- The temperature ranges of the above determined stages can be compared with the known decomposition temperature ranges of biomass waste constituents in order to assign them to the fundamental structural components such as hemicellulose, cellulose and lignin. For instance, the main constituents of OP are hemicellulose, cellulose, lignin and pectin whereas PP is mainly composed of hemicellulose, cellulose, lignin and starch. Hemicellulose, cellulose, lignin, pectin and starch are known to thermally decompose at the temperature ranges of 200–260°C, 240–350°C [40], 150–900°C [41], 233–263°C [42] and 269–345°C [43]. Comparing these known temperature ranges with the above determined temperature ranges of stages, the second stage of OP pyrolysis can be attributed to the thermal decomposition of hemicellulose and pectin

whereas the third stage of OP pyrolysis can be assigned to the thermal decomposition of cellulose. Likewise, second stage of PP pyrolysis can be attributed to the thermal decomposition of hemicellulose, cellulose and starch. Fourth stage of OP and third stage of PP were found to be due to the thermal decomposition of lignin, which decomposes over a wide temperature range and is known to be characterized by a prolonged tail in thermal curves. These assignments reflect the main decompositions in related steps and may also minorly include decompositions of other components. This is because the decomposition temperature intervals of the components that make up the biomass overlap. For instance, although the decomposition of lignin was mainly assigned to the last stages of OP and PP pyrolysis, it should not be missed that lignin decomposition also took place at earlier stages.

- The residual weights of OP and PP observed at 500°C were 25.55% and 29.19%, respectively. At 650°C, the final residual weights of OP and PP were read as 23.64% and 27.19%, respectively. Comparing the residual weights at 500°C and 650°C, it can be noticed that the difference is only about 2% indicating that the thermal decomposition was almost finished at around 500°C for both OP and PP. This can be interpreted that the main devolatilization reactions are mostly completed at around 500°C, and thus, the processes targeting bio-oil production from OP and PP should operate at least around 500°C, but further increments in pyrolysis temperature are not expected to significantly contribute to bio-oil yield since the further increased temperatures fall into the fourth stage, lignin decomposition, which is mainly responsible for char formation.

The characteristic properties of active pyrolysis stages were carefully examined for all studied heating rates since these stages were subjected to kinetic calculations. The characteristic properties included characteristic temperatures (T_i—starting temperature, T_f—ending temperature, T_{max}—the temperature at which maximum mass loss rate occurred) and maximum mass loss rate (W_{max}). The results are presented in Table 2. As can be observed clearly, all of the characteristic temperature values observed for active pyrolysis stages of OP and PP demonstrated an increase with increasing heating rate. This is in fact due to the relatively low heat conductivity of biomasses. As the biomass materials are heated with an increased heating rate, the temperature difference between the surface and the inner part of biomass particles increases due to the relatively low heat conductivity of biomass, yielding the temperature of surface higher than the inner parts. Thus, pyrolysis reactions proceed in higher temperature, which is observed as a shift of characteristic temperatures to higher values. All W_{max} values observed for active pyrolysis stages of OP and PP also demonstrated an increase with increasing heating rate as the amount of energy loaded into the system per unit time increased by increasing the heating rate. On the other hand, increasing heating rate did not significantly affect the mass loss of active pyrolysis stages, and the mass losses remained almost constant with increasing heating rate. It can be said that the time provided was high enough, even at the highest studied heating rate, so that the active pyrolysis stages were completed. On the contrary, the heating rate had an influence on the residual amounts obtained at the end of the pyrolysis process as can be observed from TG curves of PP (Fig. 1). The residual amounts obtained at 10 and 15°C/min were significantly lower than that of 2°C/min for PP (Fig. 1b). This can be related to the reduction of secondary reactions leading to a lower amount char production as the time of pyrolysis process is shortened by the increase in heating rate [44]. However, the same situation was not observed for OP, and the residual amounts remained nearly constant as can be seen from Fig. 1a.

Table 2 Properties of active pyrolysis stages of OP and PP

Property	Heating rate (°C/min)					
	2		10		15	
	S_2[a]	S_3[b]	S_2	S_3	S_2	S_3
OP						
T_i (°C)	149	246	162	260	178	274
T_f (°C)	246	347	260	367	274	382
T_{max} (°C)	186	313	208	338	218	349
W_{max} (%/min)	0.89	0.69	4.95	3.12	7.34	4.85
Mass loss (%)	26.24	22.52	27.53	23.31	27.18	22.52
PP						
T_i (°C)	231	-	250	-	260	-
T_f (°C)	323	-	329	-	344	-
T_{max} (°C)	265	-	290	-	299	-
W_{max} (%/min)	1.57	-	8.59	-	12.97	-
Mass loss (%)	36.30	-	39.43	-	40.49	-

[a] Second stage; [b] Third stage

3.3 Calculation of kinetic parameters

The kinetic parameters related to active pyrolysis stages of OP and PP were calculated by both model-free (isoconversional) and model-fitting methods including differential and integral ones, namely, FR, KAS, DAP and CR methods.

Considering Eq. 11 for calculations to be made within the scope of FR method, $\ln\left(\beta\frac{d\alpha}{dT}\right)$ versus $\frac{1}{T}$ graphs of PP and OP were plotted at heating rates of 2, 10 and 15°C/min for conversions between 0.1 and 0.9 (Fig. 2). The fitted equations, correlation coefficients (R^2) of fitted equations and the E_a values calculated from the slopes of fitted equations are given in Table 3.

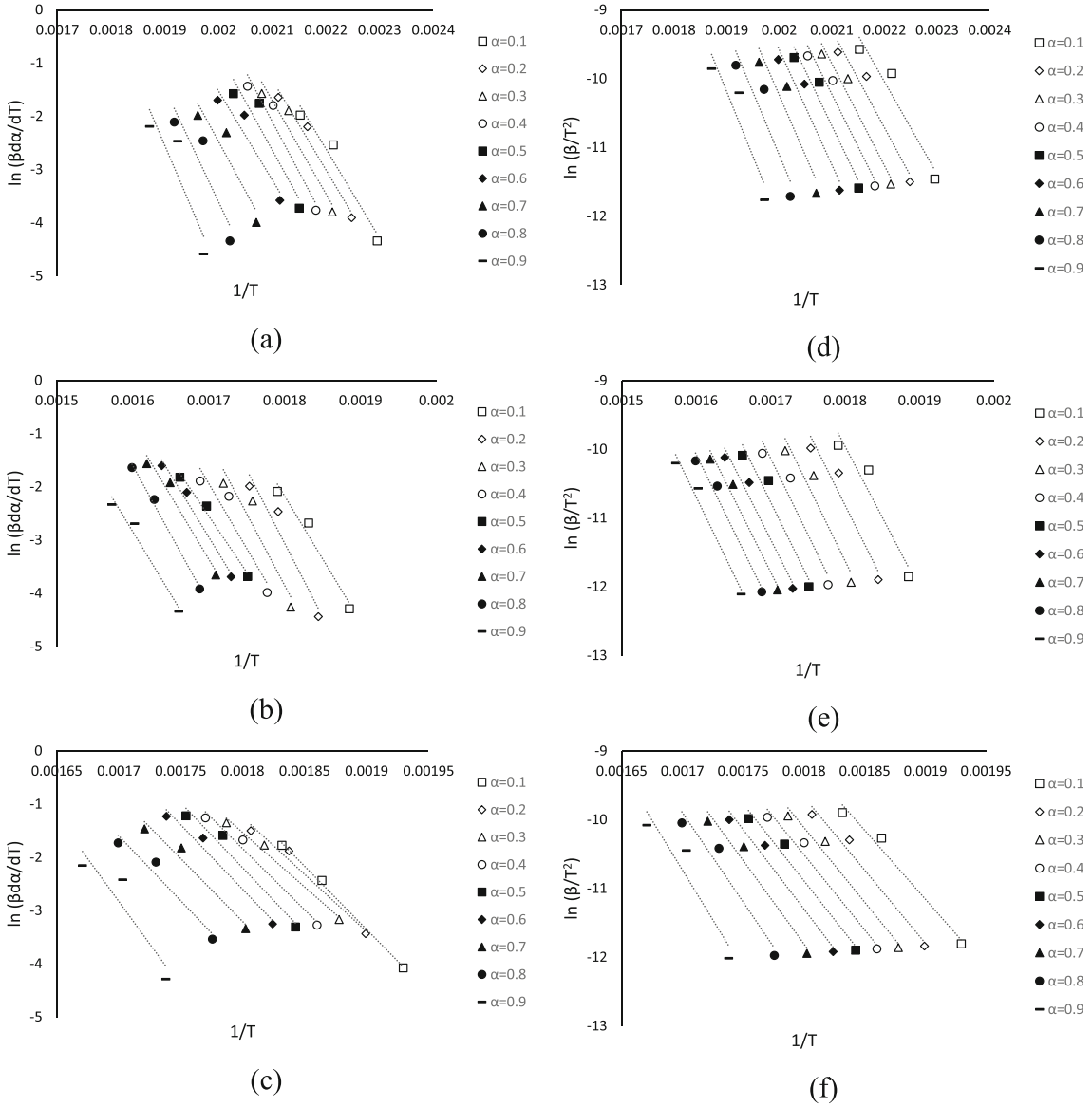

Fig. 2 $\ln\left(\beta\frac{d\alpha}{dT}\right)$ versus $\frac{1}{T}$ graphs plotted for FR method. **a** Second stage of OP pyrolysis. **b** Third stage of OP pyrolysis. **c** Second stage of PP pyrolysis; $\ln\left(\frac{\beta}{T^2}\right)$ versus $\frac{1}{T}$ graphs plotted for KAS method. **d** Second stage of OP pyrolysis. **e** Third stage of OP pyrolysis. **f** Second stage of PP pyrolysis

The calculations of KAS method were carried out according to Eq. 12. $\ln\left(\frac{\beta}{T^2}\right)$ versus $\frac{1}{T}$ graphs of PP and OP were plotted at three different heating rates (2, 10 and 15°C/min) for 0.1–0.9 conversion range (Fig. 2). The fitted equations, correlation coefficients (R^2) of fitted equations and E_a values calculated from the slopes of fitted equations are given in Table 3.

The results obtained from isoconversional methods (Table 3) indicated that the activation energy was strongly affected by the extent of conversion. For instance, having examined the results of KAS method, it was observed that increasing the extent of conversion caused a continuous increase in the E_a values for the active pyrolysis stages of both OP and PP. However, the increment observed for the third stage of OP was significantly lower than those observed for the second stages of OP and PP. When the E_a values calculated by the FR method were examined, a fluctuating and irregular behaviour was noticed with increasing extent of the conversion for all active pyrolysis stages. This behaviour can be considered as an indicator for the appearance of complex multi-step reactions including parallel, competitive and consecutive reactions [10]. In addition to this, the fluctuations observed for the active pyrolysis stages of OP were found more intense and more in numbers than that of PP indicating the occurrence of more complex reactions in the pyrolysis of OP.

If the results presented in Table 3 are examined, it can be noticed that the average E_a values calculated by FR method were higher than the average E_a values calculated by KAS method for all active pyrolysis stages of both OP and PP. It

Table 3 Kinetic parameters of OP and OP active pyrolysis stages calculated by FR and KAS methods

α	2nd stage of OP pyrolysis			3rd stage of OP pyrolysis			2nd stage of PP pyrolysis		
	R^2	Fitted equation	E_a (kJ/mol)	R^2	Fitted equation	E_a (kJ/mol)	R^2	Fitted equation	E_a (kJ/mol)
FR method									
0.1	0.9552	$y = -16766x + 34.279$	139.39	0.9666	$y = -23613x + 40.330$	196.32	0.9979	$y = -23750x + 41.771$	197.46
0.2	0.9712	$y = -16866x + 34.103$	140.22	0.9423	$y = -27634x + 46.681$	229.75	0.9785	$y = -21504x + 37.462$	178.78
0.3	0.9382	$y = -17567x + 35.192$	146.05	0.9047	$y = -26951x + 44.662$	224.07	0.9868	$y = -20481x + 35.331$	170.28
0.4	0.9458	$y = -18960x + 37.722$	157.63	0.9057	$y = -24428x + 39.594$	203.09	0.9810	$y = -23013x + 39.587$	191.33
0.5	0.8999	$y = -18310x + 35.821$	152.23	0.9867	$y = -21135x + 33.385$	175.72	0.9712	$y = -24485x + 41.877$	203.57
0.6	0.9116	$y = -16647x + 31.767$	138.40	0.9827	$y = -23401x + 36.842$	194.56	0.9762	$y = -24300x + 41.138$	202.03
0.7	0.8776	$y = -18556x + 34.639$	154.27	0.9684	$y = -23890x + 37.255$	198.62	0.9660	$y = -23721x + 39.489$	197.22
0.8	0.8485	$y = -21336x + 39.062$	177.39	0.9949	$y = -25997x + 40.000$	216.14	0.9528	$y = -24394x + 39.874$	202.81
0.9	0.8195	$y = -23673x + 42.430$	196.82	0.9699	$y = -23588x + 34.901$	196.11	0.8566	$y = -32024x + 51.614$	266.25
Avg.	0.9075		155.82	0.9580		203.82	0.9630		201.08
KAS method									
0.1	0.9308	$y = -13455x + 19.561$	111.86	0.9297	$y = -20630x + 27.174$	171.52	0.9790	$y = -20090x + 27.014$	167.03
0.2	0.9490	$y = -14202x + 20.530$	118.08	0.9393	$y = -21596x + 28.056$	179.55	0.9778	$y = -21271x + 28.618$	176.85
0.3	0.9577	$y = -14833x + 21.367$	123.32	0.9299	$y = -22095x + 28.145$	183.70	0.9767	$y = -21712x + 28.967$	180.51
0.4	0.9606	$y = -15303x + 21.909$	127.23	0.9330	$y = -22156x + 27.531$	184.21	0.9773	$y = -21917x + 28.944$	182.22
0.5	0.9524	$y = -15911x + 22.729$	132.28	0.9524	$y = -22004x + 26.637$	182.94	0.9769	$y = -22373x + 29.384$	186.01
0.6	0.9324	$y = -16760x + 23.943$	139.34	0.9673	$y = -21529x + 25.286$	178.99	0.9737	$y = -23085x + 30.255$	191.93
0.7	0.8918	$y = -17576x + 24.912$	146.13	0.9757	$y = -21671x + 25.053$	180.17	0.9664	$y = -24278x + 31.893$	201.85
0.8	0.8674	$y = -18268x + 25.430$	151.88	0.9793	$y = -22055x + 25.213$	183.37	0.9485	$y = -26027x + 34.347$	216.39
0.9	0.8682	$y = -18864x + 25.658$	156.84	0.9746	$y = -22322x + 25.022$	185.59	0.8988	$y = -28972x + 38.518$	240.87
Avg.	0.9234		134.11	0.9535		181.12	0.9639		193.74

can be seen that the same situation is also valid for most of the E_a values obtained on the basis of conversion, except for a few cases. The variations between the average E_a calculated by FR and KAS methods for second stage of OP, third stage of OP and second stage of PP were around 16.2%, 12.5% and 4.2%, respectively. Considering these values, it can be said that the results calculated by FR and KAS methods are comparatively agreeable with each other.

The high E_a values calculated by either FR or KAS methods at 0.9 conversion value for second stage of PP pyrolysis attracted considerable attention (Table 3). These high E_a values obtained at 0.9 conversion can be attributed to the need for high energy to stabilize char intermediates [31]. This was not the case for the third stage of OP pyrolysis since the E_a values calculated by FR and KAS methods for 0.9 conversion value at this stage were not high.

A comparison of average and conversion-based activated energies calculated by FR and KAS methods for second and third stages of OP pyrolysis revealed that all the values calculated for third stage were higher than that of second stage (Table 3). This may be associated with the thermal stability of the components decomposed in relevant stages. The second stage of OP pyrolysis was mainly related to the thermal decomposition of hemicellulose and pectin whereas the third stage of OP pyrolysis was mainly attributed to cellulose decomposition. The result of mentioned comparison can be considered reasonable as thermal decomposition of cellulose is completed at higher temperatures, and, thus, it is thermally more stable than hemicellulose and pectin.

Arenas et al. [10] determined the E_a values of pyrolysis kinetics of orange peel between 150 and 270 kJ/mol for the conversion range of 0.1–0.8 by using KAS, FWO, Starink, Vyazovkin and FR methods. Similarly, Kim et al. [31] calculated the E_a values of *Citrus sinensis* peel corresponding to 0.1–0.8 conversion range as 120–250 kJ/mol by using Ozawa method. In another study [30], researchers investigated the pyrolysis kinetics of orange pulp by using FR and KAS methods, and reported the E_a values between 120 and 250 kJ/mol. Ozawa-Flynn-Wall was another method used by De Morais et al. [28] to calculate E_a of OP as 92.6 kJ/mol. Finally, Santos et al. [27] determined the E_a values of OP at three peak points as 130, 145 and 229 kJ/mol by using non-isothermal Kissinger method. It can be observed that the E_a values of present study obtained by using FR and KAS methods (Table 3) coincided with the E_a values reported by the references stated above. Therefore, it can be said that E_a values

concordant with the literature data were calculated for OP. However, it is worth to mention that, the highest E_a values obtained by using FR and KAS methods in the present study were lower compared to the values reported in abovementioned references. This situation is thought to be due to the structural differences of OPs as the oranges were planted in different geographical regions.

In DAP method (Eq. 13), the appropriate selection of n is based on statistical approach, where several n values are selected, several $\ln\left(\frac{d\alpha}{dT}\right)-n\ln(1-\alpha)$ versus $\frac{1}{T}$ graphs are plotted by using selected n values and finally, determination of the plot with highest correlation coefficient (R^2) to obtain the appropriate n. For this purpose, several values of n were selected, several $\ln\left(\frac{d\alpha}{dT}\right)-n\ln(1-\alpha)$ versus $\frac{1}{T}$ graphs were plotted by using selected n values and the correlation coefficients (R^2) of these plots were calculated to generate $R^2 - n$ curves (Fig. 3). The most appropriate n, i.e. the n value providing the highest R^2 value, was determined from the generated $R^2 - n$ curves. Then, using the determined n values, final $\ln\left(\frac{d\alpha}{dT}\right)-n\ln(1-\alpha)$ versus $\frac{1}{T}$ graphs (Fig. 4) were plotted to calculate activation energies and pre-exponential factors. The results are presented in Table 4. It must be mentioned that kinetic parameters for 2°C/min heating rate could not be calculated since the final $\ln\left(\frac{d\alpha}{dT}\right)-n\ln(1-\alpha)$ versus $\frac{1}{T}$ graphs drawn by using the most appropriate n values (determined from the maximum point of $R^2 - n$ plots) were curves instead of straight lines. Thus, it was concluded that DAP method may not be suitable for determining reaction order (and other kinetic parameters)

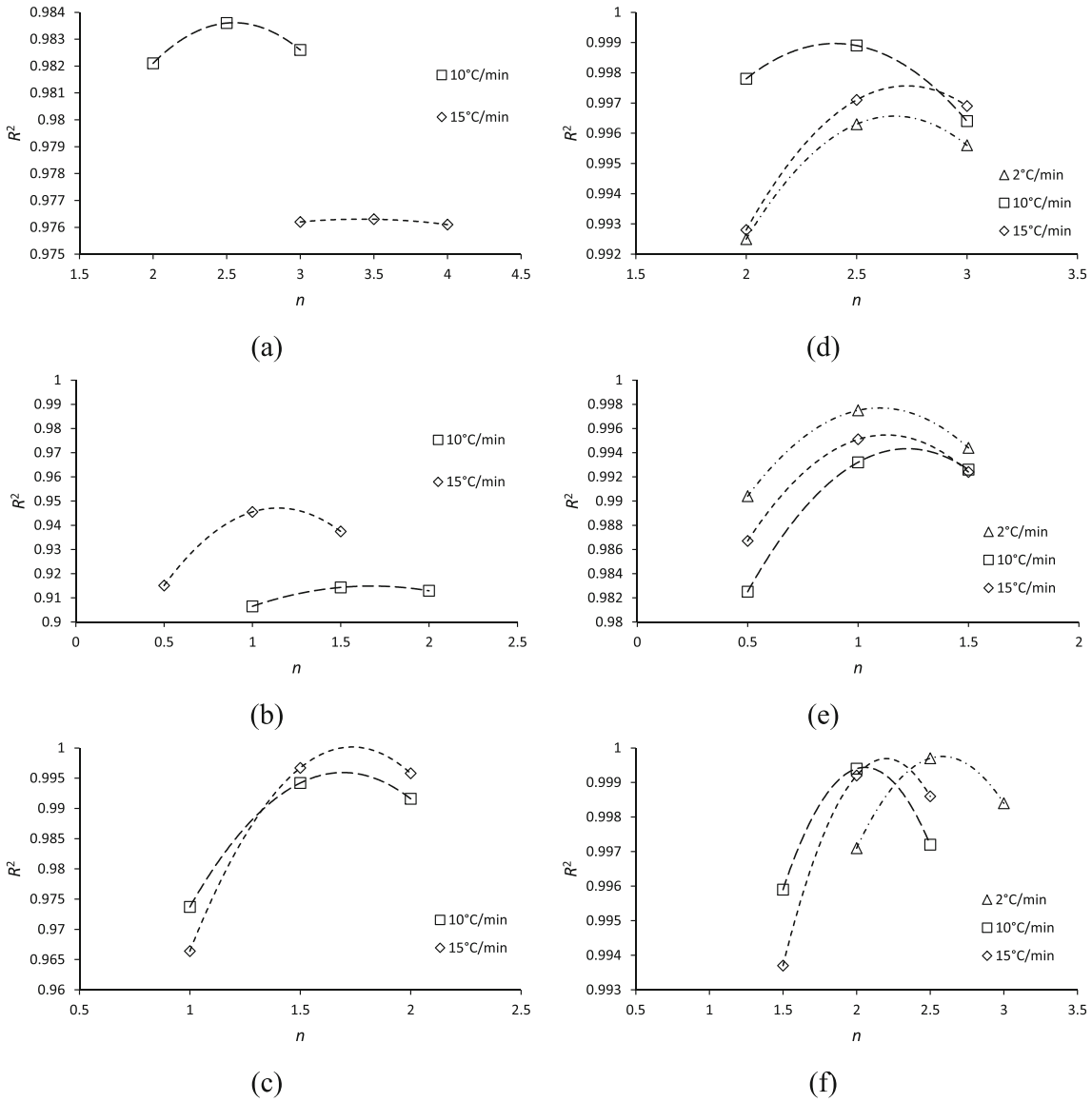

Fig. 3 $R^2 - n$ graphs generated for DAP method. **a** Second stage of OP pyrolysis. **b** Third stage of OP pyrolysis. **c** Second stage of PP pyrolysis; for CR method. **d** Second stage of OP pyrolysis. **e** Third stage of OP pyrolysis. **f** Second stage of PP pyrolysis

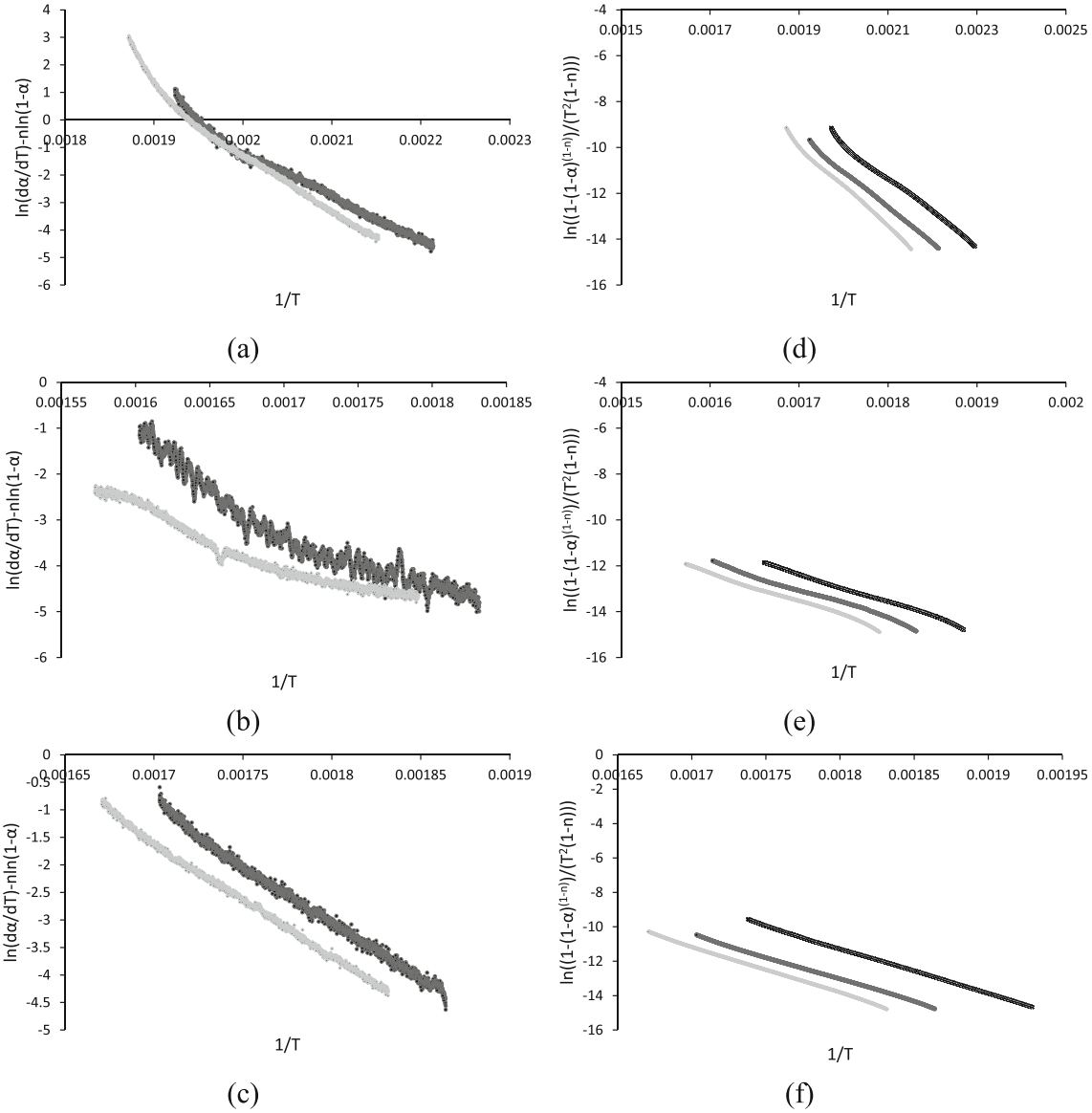

Fig. 4 Final $\ln\left(\frac{d\alpha}{dT}\right)-n\ln(1-\alpha)$ versus $\frac{1}{T}$ graphs generated for DAP method. **a** Second stage of OP pyrolysis. **b** Third stage of OP pyrolysis. **c** Second stage of PP pyrolysis; final $\ln\left(\frac{1-(1-\alpha)^{1-n}}{T^2(1-n)}\right)$ versus $\frac{1}{T}$ graphs generated for CR method. **d** Second stage of OP pyrolysis. **e** Third stage of OP pyrolysis. **f** Second stage of PP pyrolysis (black square—2°C/min, dark grey circle—10°C/min, light grey diamond—15°C/min)

from thermogravimetric data obtained at very slow heating rates such as 2°C/min by applying the method described above.

In CR method (Eqs. 14 and 15), several n values are selected, several left hand side of Eqs. 14 and 15 versus 1/T graphs are plotted by using the selected n values and finally, the plot having the highest correlation coefficient (R^2) is specified to determine the most appropriate n value. Thus, several values of n were selected, several left hand side of Eqs. 14 and 15 versus 1/T graphs were plotted by using selected n values and the correlation coefficients (R^2) of these plots were calculated to generate $R^2 - n$ curves (Fig. 3). The most appropriate n, i.e. the n value providing the highest R^2 value, was determined from the generated $R^2 - n$ curves. Then, using the determined n values, the final left hand side of Eq. 14 or 15 versus 1/T graphs (Fig. 4) were plotted to calculate activation energies and pre-exponential factors. The results are listed in Table 4.

The results given in Table 4 were examined, and the variations between the average E_a values calculated by DAP and CR methods for second stage of OP, third stage of OP and second stage of PP pyrolysis processes were determined as app. 28%, 11.2% and 25.5%, respectively, which were significantly higher than the variations determined between FR and KAS results.

For pyrolysis of OP, all kinetic parameters calculated by DAP method, except for the E_a calculated at 15°C/min heating rate for the third stage, were significantly higher than the kinetic parameters calculated by CR method (Table 4).

Table 4 Kinetic parameters of OP and PP active pyrolysis stages calculated by CR and DAP methods

β (°C/min)	Stage	E_a (kJ/mol)	A (1/s)	Fitted equation	R^2	n
CR method						
OP						
2	2nd	120.68	9.8150E+10	$y = -14515x + 19.128$	0.9964	2.67
	3rd	101.41	1.7587E+06	$y = -12198x + 8.3723$	0.9976	1.10
10	2nd	129.48	1.4071E+12	$y = -15574x + 20.111$	0.9991	2.40
	3rd	100.87	3.9321E+06	$y = -12132x + 7.5728$	0.9942	1.22
15	2nd	144.78	4.9093E+13	$y = -17414x + 23.146$	0.9974	2.73
	3rd	103.36	6.0607E+06	$y = -12432x + 7.5756$	0.9953	1.13
Average	2nd	131.65	1.6866E+13			2.60
	3rd	101.88	3.9172E+06			1.15
PP						
2	2nd	216.64	2.5995E+18	$y = -26057x + 35.635$	0.9997	2.58
10	2nd	212.95	9.7783E+17	$y = -25613x + 33.065$	0.9994	2.06
15	2nd	224.04	7.6203E+18	$y = -26947x + 34.662$	0.9995	2.20
Average	2nd	217.88	3.7325E+18			2.28
DAP method						
OP						
10	2nd	143.62	5.9633E+13	$y = -17275x + 33.511$	0.9836	2.55
	3rd	128.81	2.0564E+09	$y = -15493x + 23.236$	0.9142	1.67
15	2nd	193.43	1.3372E+19	$y = -23266x + 45.426$	0.9763	3.42
	3rd	97.70	2.2664E+06	$y = -11751x + 16.020$	0.9440	1.14
Average	2nd	168.53	6.6860E+18			2.99
	3rd	113.26	1.0293E+09			1.41
PP						
10	2nd	174.01	1.8186E+14	$y = -20930x + 34.626$	0.9940	1.69
15	2nd	173.10	1.1931E+14	$y = -20818x + 33.799$	0.9973	1.74
Average	2nd	173.56	1.5059E+14			1.72

However, for the second stage of PP pyrolysis, just the opposite case was observed, i.e. all the kinetic parameters calculated by CR method were higher than the kinetic parameters calculated by DAP method.

Having compared the values calculated for the second and third stages of OP pyrolysis (Table 4), it was noticed that all E_a values related to third stage calculated by both DAP and CR methods were lower than the E_a values calculated for second stage by the same methods. This was the opposite of the situation encountered in isoconversional (FR and KAS) calculations. The expected situation was not observed since the third stage was mainly due to decomposition of cellulose which is thermally more stable than hemicellulose and pectin, the components whose decomposition mainly took place in second stage.

Average E_a results calculated by CR, DAP, FR and KAS methods were compared to determine the consistency of the results. The values calculated for the second stage of OP pyrolysis were in the range of 131.65–168.53 kJ/mol. For the second stage of PP pyrolysis, the results lied between 173.56 and 217.88 kJ/mol. It would be righteous to mention that the results calculated by all studied methods in these two active pyrolysis stages were relatively concordant. For the third stage of OP pyrolysis, the results calculated by isoconversional methods were agreeable with each other (181.12, 203.81 kJ/mol), and model-fitting methods gave consistent results among themselves (101.88, 113.26 kJ/mol). However, when the results calculated by all studied methods were evaluated together, the differences between these two method groups (i.e. isoconversional and model-fitting) were found evidently high. The results calculated from distinct methods were expected to vary due to the different approaches used in derivation of the methods. However, the differences determined for the third stage of OP pyrolysis were considerably higher than expected.

The E_a value of pyrolysis process represents the minimum energy amount that must be provided for pyrolysis reactions to take place. For this reason, the E_a values of OP and PP calculated within the scope of present study were compared with the E_a values of several types of biomass including corn stover (179.6, 207.4 and 239.3 kJ/mol), cotton stalk (178.2, 205.3 and 239.5 kJ/mol), palm oil husk (169.7, 200 and 236.1

kJ/mol), pine wood (186.7, 214.4 and 271.76 kJ/mol), red oak (183.1, 209.6 and 242.1 kJ/mol), sugar cane bagasse (184.8, 212.5 and 234.8 kJ/mol), switch grass (186.8, 212.1 and 261 kJ/mol), wheat straw (175.5, 204.2 and 240.6 kJ/mol) [45], corn brakes (300.6 kJ/mol) hazelnut shell (216.35 kJ/mol), beech sawdust (227.8 kJ/mol), MDF sawdust (260.7 kJ/mol) [46], brewery spent grains (218, 221 and 213 kJ/mol), coffee waste (236, 222 and 224 kJ/mol) [47], microalgae—*Spirulina platensis* (153.2 kJ/mol) and swine manure digestate (209.5 kJ/mol) [48]. The comparison revealed that the average E_a values calculated for OP and PP in the present study (Tables 3 and 4) are around typical biomass E_a values. Thus, pyrolysis processes of OP and PP are expected to require energy amounts similar to the ones that are provided for pyrolysis processes of many biomass types.

The reaction order (n) and pre-exponential factor (A) were the other kinetic parameters calculated by DAP and CR methods. DAP and CR methods yielded average reaction order for the second stage of OP pyrolysis as 2.99 and 2.60, respectively. The same results for the third stage of OP pyrolysis were calculated as 1.41 and 1.15 by DAP and CR methods, respectively. The average reaction orders calculated for the second stage of PP pyrolysis by DAP and CR methods were 1.72 and 2.28, respectively. So, comparing the average reaction orders, it can be said that both DAP and CR methods yielded relatively close results, especially for OP. However, as can be observed from Table 3, pre-exponential factors calculated by DAP and CR methods were not close and differed in orders of magnitude.

4 Conclusion

The thermogravimetric analyses were carried out to determine the pyrolysis characteristics and kinetics of OP and PP. The thermal decompositions of OP and PP were shown to occur in four and three stages respectively. It was observed that OP and PP completed their decompositions almost at 500°C with 74.45% and 70.81% conversion based on volatiles, respectively. This is an important indicator that OP and PP can be promising candidate raw materials for pyrolysis processes aiming liquid products since the volatiles that are rapidly cooled down constitute the major part of liquid products. The kinetic parameters essential for the design, optimization and scaling of pyrolysis process, were calculated by CR, DAP, FR and KAS methods. The average E_a values calculated for OP and PP revealed that the pyrolysis processes of OP and PP require typical energy amounts observed for many types of biomass. The DAP method, as applied here, was not found appropriate to calculate the kinetic parameters at very slow heating rates (e.g. 2°C/min).

Acknowledgements The author would like to thank Dr. Gözde Gözke Açıkalın for her continuous support during the studies.

References

1. Kannan N, Vakeesan D (2016) Solar energy for future world: - a review. Renew Sust Energ Rev 62:1092–1105. https://doi.org/10.1016/j.rser.2016.05.022
2. Kan S, Chen B, Chen G (2019) Worldwide energy use across global supply chains: decoupled from economic growth? Appl Energy 250:1235–1245. https://doi.org/10.1016/j.apenergy.2019.05.104
3. Kan SY, Chen B, Wu XF, Chen ZM, Chen GQ (2019) Natural gas overview for world economy: from primary supply to final demand via global supply chains. Energy Policy 124:215–225. https://doi.org/10.1016/j.enpol.2018.10.002
4. Bermúdez CA, Porteiro J, Varela LG, Chapela S, Patiño D (2020) Three-dimensional CFD simulation of a large-scale grate-fired biomass furnace. Fuel Process Technol 198:106219. https://doi.org/10.1016/j.fuproc.2019.106219
5. Varma AK, Singh S, Rathore AK, Thakur LS, Shankar R, Mondal P (2020) Investigation of kinetic and thermodynamic parameters for pyrolysis of peanut shell using thermogravimetric analysis. Biomass Conversion and Biorefinery. https://doi.org/10.1007/s13399-020-00972-y
6. Kothandaraman MP, Somasundaram M (2019) Non-isothermal kinetic study on copyrolysis of Juliflora and low-density polyethylene. Biomass Conversion and Biorefinery. https://doi.org/10.1007/s13399-019-00559-2
7. Ahmad MS, Mehmood MA, Taqvi STH, Elkamel A, Liu CG, Xu J, Rahimuddin SA, Gull M (2017) Pyrolysis, kinetics analysis, thermodynamics parameters and reaction mechanism of *Typha latifolia* to evaluate its bioenergy potential. Bioresour Technol 245(Part A): 491–501. https://doi.org/10.1016/j.biortech.2017.08.162
8. Şen AU, Fonseca FG, Funke A, Pereira H, Lemos F (2020) Pyrolysis kinetics and estimation of chemical composition of *Quercus cerris* cork. Biomass Conversion and Biorefinery. https://doi.org/10.1007/s13399-020-00964-y
9. Cai J, Xu D, Dong Z, Yu X, Yang Y, Banks SW, Bridgwater AV (2018) Processing thermogravimetric analysis data for isoconversional kinetic analysis of lignocellulosic biomass pyrolysis: case study of corn stalk. Renew Sust Energ Rev 82(3):2705–2715. https://doi.org/10.1016/j.rser.2017.09.113
10. Arenas CN, Navarro MV, Martínez JD (2019) Pyrolysis kinetics of biomass wastes using isoconversional methods and the distributed activation energy model. Bioresour Technol 288:121485. https://doi.org/10.1016/j.biortech.2019.121485
11. Özsin G, Pütün AE (2019) TGA/MS/FT-IR study for kinetic evaluation and evolved gas analysis of a biomass/PVC co-pyrolysis process. Energy Convers Manag 182:143–153. https://doi.org/10.1016/j.enconman.2018.12.060
12. Ma Z, Chen D, Gu J, Bao B, Zhang Q (2015) Determination of pyrolysis characteristics and kinetics of palm kernel shell using TGA–FTIR and model-free integral methods. Energy Convers Manag 89:251–259. https://doi.org/10.1016/j.enconman.2014.09.074
13. Amini E, Safdari MS, Weise DR, Fletcher TH (2019) Pyrolysis kinetics of live and dead wildland vegetation from the Southern United States. J Anal Appl Pyrolysis 142:104613. https://doi.org/10.1016/j.jaap.2019.05.002
14. Christoforou E, Fokaides PA (2016) A review of olive mill solid wastes to energy utilization techniques. Waste Manag 49:346–363. https://doi.org/10.1016/j.wasman.2016.01.012
15. Pathak PD, Mandavgane SA, Kulkarni BD (2017) Fruit peel waste: characterization and its potential uses. Curr Sci 113(3):444-454. https://doi.org/10.18520/cs/v113/i03/444-454
16. Torre I, Martin-Dominguez V, Acedos MG, Esteban J, Santos VE, Ladero M (2019) Utilisation/upgrading of orange peel waste from a biological biorefinery perspective. Appl Microbiol Biotechnol 103: 5975–5991. https://doi.org/10.1007/s00253-019-09929-2

17. Siles JA, Vargas F, Gutiérrez MC, Chica AF, Martín MA (2016) Integral valorisation of waste orange peel using combustion, biomethanisation and co-composting technologies. Bioresour Technol 211:173–182. https://doi.org/10.1016/j.biortech.2016.03.056
18. Zhang B, Chen J, He Z, Chen H, Kandasamy S (2019) Hydrothermal liquefaction of fresh lemon-peel: parameter optimisation and product chemistry. Renew Energy 143:512–519. https://doi.org/10.1016/j.renene.2019.05.003
19. Rezzadori K, Benedetti S, Amante ER (2012) Proposals for the residues recovery: orange waste as raw material for new products. Food Bioprod Process 90:606–614. https://doi.org/10.1016/j.fbp.2012.06.002
20. Negro V, Ruggeri B, Fino D, Tonini D (2017) Life cycle assessment of orange peel waste management. Resour Conserv Recycl 127:148–158. https://doi.org/10.1016/j.resconrec.2017.08.014
21. Bhatnagar A, Sillanpää M, Witek-Krowiak A (2015) Agricultural waste peels as versatile biomass for water purification – a review. Chem Eng J 270:244–271. https://doi.org/10.1016/j.cej.2015.01.135
22. De Carvalho WT, De Oliveira TF, Da Silva FA, Caliari M, Soares Júnior MS (2014) Drying kinetics of potato pulp waste. Food Science and Technology 34(1):116–122. https://doi.org/10.1590/S0101-20612014000100017
23. El-Azazy M, El-Shafie IAA, Al-Sulaiti M, Al-Yafie J, Shomar B, Al-Saad K (2019) Potato peels as an adsorbent for heavy metals from aqueous solutions: eco-structuring of a green adsorbent operating Plackett–Burman design. J Chemother 4926240:1–14. https://doi.org/10.1155/2019/4926240
24. Arampatzidou AC, Deliyanni EA (2016) Comparison of activation media and pyrolysis temperature for activated carbons development by pyrolysis of potato peels for effective adsorption of endocrine disruptor bisphenol-A. J Colloid Interface Sci 466:101–112. https://doi.org/10.1016/j.jcis.2015.12.003
25. Bernardo M, Rodrigues S, Lapa N, Matos I, Lemos F, Batista MKS, Carvalho AP, Fonseca I (2016) High efficacy on diclofenac removal by activated carbon produced from potato peel waste. Int J Environ Sci Technol 13:1989–2000. https://doi.org/10.1007/s13762-016-1030-3
26. Arapoglou D, Varzakas T, Vlyssides A, Israilides C (2010) Ethanol production from potato peel waste (PPW). Waste Manag 30:1898–1902. https://doi.org/10.1016/j.wasman.2010.04.017
27. Santos CM, Dweck J, Viotto RS, Rosa AH, de Morais LC (2015) Application of orange peel waste in the production of solid biofuels and biosorbents. Bioresour Technol 196:469–479. https://doi.org/10.1016/j.biortech.2015.07.114
28. De Morais LC, Santos CM, Rosa AH (2015) Thermodynamic parameters of a solid biofuel from orange peel. Chem Eng Trans 43:583–588. https://doi.org/10.3303/CET1543098
29. Martínez-Vargas DX, Sandoval-Rangel L, Solís-Maldonado C, De La Rosa JR, Lucio-Ortiz CJ, Dimas-Rivera G, Ramos-Delgado NA, Mendoza-Domínguez A (2018) Application of natural minerals for in-situ catalytic pyrolysis of orange peel. J Appl Res Technol 16:404-421. https://doi.org/10.22201/icat.16656423.2018.16.5.736
30. Lopez-Velazquez MA, Santes V, Balmaseda J, Torres-Garcia E (2013) Pyrolysis of orange waste: a thermo-kinetic study. J Anal Appl Pyrolysis 99:170–177. https://doi.org/10.1016/j.jaap.2012.09.016
31. Kim Y-M, Jae J, Lee HW, Han TU, Lee H, Park SH, Kim S, Watanabe C, Park Y-K (2016) Ex-situ catalytic pyrolysis of citrus fruit peels over mesoporous MFI and Al-MCM-41. Energy Convers Manag 125:277–289. https://doi.org/10.1016/j.enconman.2016.02.065
32. Liang S, Han Y, Wei L, McDonald AG (2015) Production and characterization of bio-oil and bio-char from pyrolysis of potato peel wastes. Biomass Conversion and Biorefinery 5:237–246. https://doi.org/10.1007/s13399-014-0130-x
33. Önal E, Uzun BB, Pütün AE (2012) An experimental study on bio-oil production from co-pyrolysis with potato skin and high-density polyethylene (HDPE). Fuel Process Technol 104:365–370. https://doi.org/10.1016/j.fuproc.2012.06.010
34. Önal EP, Uzun BB, Pütün AE (2011) Steam pyrolysis of an industrial waste for bio-oil production. Fuel Process Technol 92:879–885. https://doi.org/10.1016/j.fuproc.2010.12.006
35. Gupta S, Gupta GK, Mondal MK (2020) Thermal degradation characteristics, kinetics, thermodynamics, and reaction mechanism analysis of pistachio shell pyrolysis for its bioenergy potential. Biomass Conversion and Biorefinery. https://doi.org/10.1007/s13399-020-01104-2
36. Mishra RK, Mohanty K (2018) Pyrolysis kinetics and thermal behavior of waste sawdust biomass using thermogravimetric analysis. Bioresour Technol 251:63–74. https://doi.org/10.1016/j.biortech.2017.12.029
37. Pradhan RR, Garnaik PP, Regmi B, Dash B, Dutta A (2017) Pyrolysis kinetics of Sal (Shorea robusta) seeds. Biomass Conversion and Biorefinery 7:237–246. https://doi.org/10.1007/s13399-017-0240-3
38. Singh Chouhan AP, Sarma AK (2013) Critical analysis of process parameters for bio-oil production via pyrolysis of biomass: a review. Recent Pat Eng 7(2):98–114. https://doi.org/10.2174/1872212113079990005
39. Kyzas GZ, Deliyanni EA, Matis KA (2016) Activated carbons produced by pyrolysis of waste potato peels: cobalt ions removal by adsorption. Colloids Surf A Physicochem Eng Asp 490:74–83. https://doi.org/10.1016/j.colsurfa.2015.11.038
40. Mohan D, Pittman CU, Steele P (2006) Pyrolysis of wood/biomass for bio-oil: a critical review. Energy Fuel 20:848–889. https://doi.org/10.1021/ef0502397
41. Waters CL, Janupala RR, Mallinson RG, Lobban LL (2017) Staged thermal fractionation for segregation of lignin and cellulose pyrolysis products: an experimental study of residence time and temperature effects. J Anal Appl Pyrolysis 126:380–389. https://doi.org/10.1016/j.jaap.2017.05.008
42. Einhorn-Stoll U, Kunzek H (2009) Thermoanalytical characterisation of processing-dependent structural changes and state transitions of citrus pectin. Food Hydrocoll 23(1):40–52. https://doi.org/10.1016/j.foodhyd.2007.11.009
43. Xue J, Ceylan S, Goldfarb JL (2015) Synergism among biomass building blocks? Evolved gas and kinetics analysis of starch and cellulose co-pyrolysis. Thermochim Acta 618:36–47. https://doi.org/10.1016/j.tca.2015.09.002
44. Qiao Y, Wang B, Ji Y, Xu F, Zong P, Zhang J, Tian Y (2019) Thermal decomposition of castor oil, corn starch, soy protein, lignin, xylan, and cellulose during fast pyrolysis. Bioresour Technol 278:287–295. https://doi.org/10.1016/j.biortech.2019.01.102
45. Wu W, Mei Y, Zhang L, Liu R, Cai J (2014) Effective activation energies of lignocellulosic biomass pyrolysis. Energy Fuel 28:3916–3923. https://doi.org/10.1021/ef5005896
46. Radojević M, Janković B, Jovanović V, Stojiljković D, Manić N (2018) Comparative pyrolysis kinetics of various biomasses based on model-free and DAEM approaches improved with numerical optimization procedure. PLoS One 13(10):e0206657. https://doi.org/10.1371/journal.pone.0206657
47. Becidan M, Várhegyi G, Hustad JE, Skreiberg Ø (2007) Thermal decomposition of biomass wastes. A kinetic study. Ind Eng Chem Res 46:2428–2437. https://doi.org/10.1021/ie061468z
48. Vuppaladadiyam AK, Liu H, Zhao M, Soomro AF, Memon MZ, Dupont V (2019) Thermogravimetric and kinetic analysis to discern synergy during the co-pyrolysis of microalgae and swine manure digestate. Biotechnology for Biofuels 12:170. https://doi.org/10.1186/s13068-019-1488-6